International Journal of Oceans and Oceanography
ISSN 0973-2667 Volume 12, Number 2 (2018), pp. 147-158

http://www.ripublication.com

Ocean Surface Winds from Aquarius L-band Radiometer during Tropical Cyclones: Case Studies

Abhineet Shyam and Neerja Sharma

Geophysical parameters Retrieval Division, Atmospheric and Oceanic Sciences Group, EPSA, Space Applications Centre, ISRO, Ahmedabad-58, Gujarat, India.

ABSTRACT

The paper presents a demonstrative study towards utilizing L-band (1.4 GHz) microwave radiometric observations of ocean surface emission for deriving high wind speeds (WS) prevailing during tropical cyclones. The study also establishes the wind geophysical model function (GMF), which is developed from simulations of brightness temperature (BT) of ocean surface for the real cases of tropical cyclones (TCs) using the radiative transfer model. Simulation parameters such as the observation frequency, incidence angle and noise equivalent delta temperature (NEDT) are tuned in the model to match AQUARIUS mission specifications for L-band radiometer. The behavior of simulated BT with WS is bilinear over two wind regimes. The wind GMF is based on a bivariate regression model establishing the linear relationship between BT and WS and is applied on cyclonic cases of NURI and NILOFAR and the spatial variations of BT with high WS conditions are found to be well captured. Scatterplot for estimated WS shows a consistent performance over high wind range of 12 m/s to 32 m/s for NURI and NILOFAR with correlation coefficient of 0.83 and standard deviations within 3.1 m/s.

1. INTRODUCTION

Monitoring the ocean surface wind of tropical cyclones (TCs) forming over tropical oceans is extremely important from operational and scientific points of view. TC track and intensity forecasts by TC forecast models demand precise initial conditions of air and sea states for improving their skills of forecast. Past efforts for direct measurement of ocean surface wind field could not meet the stringent requirements of synoptic global wind fields as dictated by these forecast models. Mostly, these direct measurements of ocean surface wind came from merchant ships and in-situ buoys and they, as stated, had simply insufficient spatio-temporal coverage. Needless to say, however, that direct measurements of ocean wind offer valuable data for research and validation of satellite-

derived winds. Satellite measurements of ocean surface wind by microwave scatterometer/radiometer can provide spatio-temporal coverage much better than in-situ observations. Scatterometer/radiometer wind products are more informative as they provide along with wind magnitude, the direction of ocean surface winds, but only under non-raining conditions [1], [2], [3]. Severe limitation is posed to the accuracy of scatterometer winds under raining conditions, reducing thus, the effectiveness of such instruments for extreme convective events like TCs, which are often accompanied by intense rainfall. Ocean winds have been derived from altimeter and synthetic aperture radar measurements as secondary products as these instruments are primarily not meant for wind measurements. Thus, they can neither be used operationally nor for a wide range of research purposes due to their limited coverage and accuracy. Space-borne passive microwave instrument, commonly called a microwave radiometer (MR), with C-band to Ka-band frequencies have been used since many years for the remote sensing of the oceans and atmosphere. They normally operate in multi-frequency and dual linear polarized channels, making simultaneous observations of microwave emissivity at multiple channels for retrieval of atmospheric and oceanic parameters such as water vapour, cloud liquid water, rain rate, sea surface temperature (SST) and near surface wind speed (WS). But, they are constrained by the reduced sensitivity to hurricane force winds and by the inaccuracy caused by the impact of rain. From the sensitivity analyses of emissivity at different ocean WS for various microwave frequency bands and with further incorporation of the knowledge of rain attenuation of microwave emissions at different microwave frequencies [4], it is found that remote sensing of ocean surface winds at L-band is highly sensitive to extreme weather conditions over oceans during TCs. The effect of rain on L-band observations of emissivity is also negligible.

When the sea becomes rough due to higher WS and in the presence of sea foam, the change in reflectivity or emissivity causes the L-band microwave radiometer BT to increase [5]. At L-band, the sensitivity to combined contributions of sea foam and roughness induced emissivity increases at higher WS, showing the desirability of using an L-band radiometer for ocean surface WS retrieval in extreme weather conditions during TCs. Also, an Earth-looking L-band radiometer will observe the sea surface brightness without much loss from atmospheric attenuation. The effect of rain from low to high rain rate and ice clouds attenuation on L-band radiation is also negligible. The specific attenuation which is the attenuation loss per unit length of propagation path in units of dB/km is less than 0.01 at L-band (< 2 GHz) even at intense rain rate of 150 mm/hr [4]. The brightness sensitivity to liquid cloud and water vapour is near zero around 1-2 GHz.

Although, L-band remote sensing of oceans is relatively new, its potential as a critical gap filler for hurricane WS retrieval under severe weather systems has promisingly been demonstrated from the first space-borne L-band radiometer onboard Soil Moisture Ocean Salinity (SMOS) mission of European Space Agency (ESA) which was launched in November 2009 [6], [7]. The Aquarius mission of National Aeronautics and Space Administration (NASA), launched in June 2011, was the second L-band mission to provide accurate measurements of global ocean salinity [8]. The mission consists of three integrated, pushbroom-type polarimetric L-band radiometers at 1.41 GHz

designed and developed by NASA's Goddard Space Flight Centre (GSFC), besides an L-band scatterometer at 1.26 GHz, designed and developed by NASA's Jet Propulsion Laboratory (JPL). The advantage of a pushbroom-type over a synthetic aperture radiometer system is that it gives superior radiometric resolution with superior accuracy and stability [9]. The footprint sizes of the three radiometric beams are 76 km x 94 km, 84 km x 120 km and 96 km x 156 km with a total swath width of 390 km. The three beams are inclined at an incidence angle of 28.7^{o} (beam-1), 37.8^{o} (beam-2) and 45.6^{o} (beam-3) w.r.t. nadir. The L-band real-aperture scatterometer shares the antenna with the radiometer system. With a sun-synchronous polar orbit at 675 km altitude and node crossing time of 6 AM/6 PM, the satellite has a revisit time of 7 days with a radiometric stability of 0.12 K. [10] have demonstrated the WS retrieval from AQUARIUS radiometer using a neural network technique. [11] developed combined active-passive algorithm for the ocean surface winds estimation from Aquarius. Recently, NASA has launched in January 2015, the Soil Moisture Active Passive (SMAP) satellite which has an L-band radiometer onboard, in addition to, the L-band radar (now, non-functional) with the stated objective of measuring soil moisture at a very high spatial resolution. [12] demonstrated the estimation of wind speed and direction from SMAP L-band radiometer data using the combined geophysical model function of SMAP and Aquarius. Wind speed retrieval from SMAP L-band radiometer was also documented by [13] and [14]. The radiometric accuracy of microwave radiometer aboard SMOS, AQUARIUS and SMAP is ~1.5 K [15], < 0.15 K [16] and < 1 K [17], respectively. Among the three missions, this paper demonstrates the WS retrieval on Aquarius L-band radiometer, primarily, because of the relatively good radiometric accuracy than other two missions. However, the limited swath (390 Km) does not permit to locate complete structure of the TC.

2. DATA USED

AQUARIUS Level-2, version-4, data products were used in the study from the period 20^{th} October, 2014 to 10^{th} November, 2014. Brightness temperature (BT) at both H-pol and V-pol for the beam-1, latitude and longitude for beam-1, date and time information and ancillary winds are extracted from each of the data files in this period. The data products are available through Physical Oceanography Distributed Active Archive Centre (PODAAC) maintained by JPL/NASA [ftp://podaac-ftp.jpl.nasa.gov/allData/Aquarius/L2/V4]. National Centre for Environmental Prediction (NCEP)'s Global Forecast System (GFS) gridded analyses fields provide the vertical profiles of temperature, relative humidity and surface parameters of WS and SST at various grid resolutions. For the radiative transfer model (RTM) simulation, 0.5^{o} spatial grid and 6 hrs daily analysed data files are downloaded and processed for simulations. The GFS data is available from www.ncdc.noaa.gov. Sea surface salinity is parametrically used in the simulation at intervals of 0.1 psu for the full dynamic range of 10 – 40 psu. The data for the period 20^{th} - 25^{th} October, 2014 (GONZALO) and 28^{th} October - 3^{rd} November, 2015 (CHAPALA) are used for the simulation of BT using RTM. The validation of the estimations is carried out with GFS analysed maximum WS during TC NURI and NILOFAR.

3. SIMULATION EXPERIMENT

Generally, the inverse model for estimation of geophysical parameters from satellites is developed from simulations of satellite measurements. [18], [19] proposed WS retrieval algorithm for Advanced Microwave Scanning Radiometer-Earth Observing System with the combined use of satellite observations and model simulations. The GMF for retrieval of WS from Aquarius radiometric BT is accordingly developed based on simulations of BT using the RTM given by [20] (here onwards, K-model). For this purpose, the model is tuned for the frequency and incidence angle of 1.41 GHz and 28.7^{o}, respectively as per the AQUARIUS specifications. The K-model is based on an Eddington approximation and the solutions are developed for time-independent, vertically inhomogeneous, non-isothermal, multi-layered plane parallel atmospheric medium [20] . It includes the physical processes of thermal emission, absorption, scattering and emission at the lower boundary. Infact, the K-model properly captures the angular distribution of radiation as any RTM should do in the case of multiple scattering of microwave radiation propagating through precipitation. The vertical profiles of temperature, relative humidity and surface parameters of SST and WS are required as input to the K-model to simulate BT. The K-model internally takes care of surface roughness [21], cosmic background radiation (2.7 K), atmospheric absorption by water vapour [22] and molecular oxygen using [23]. The errors in the calculated BT are far smaller than those introduced by the usual errors found in the input parameters. Furthermore, the computational efficiency of K-model code is roughly 20 times greater than other codes [20]. Due to the model simplicity and computational efficiency, it has been widely used for satellite remote sensing towards development of retrieval algorithm for a host of geophysical parameters sensitive to microwave frequencies.

Such a practice of using simulations for GMF development is also beneficial as the model simulations ensure accurate estimations of WS. Further, the GMF for high-wind conditions needs match-up dataset of BT from satellite and WS from in-situ or satellite derived products. Not many sources of high wind data are available and, where ever they exist, there may not be enough collocation with satellite observations. In the light of these limitations, the use of match-up data of model simulated BT with the high WS data remains a viable and reliable option.

Since the objective of this study is to estimate high wind during the TCs, selected cases of TCs are earmarked for the simulations and validation. The BT of Aquarius are simulated for the two (CHAPALA and GONZALO) TCs cases. CHAPALA cyclone originated on 28th October 2015 from 11.5 N; 65 E, reached a maximum intensity of WS of 135 kt on 31st October 2015 and dissipated on 3rd November 2015 at 14.2 N; 47.2 E. On the other hand, GONZALO originated on 12th October 2014 from 16.7 N; 57.4 W, reached a maximum intensity of WS of 125 kt on 16th October 2014 at 25.6 N; 68.7 W at 12 UTC. It sustained with WS over 100 kt till 17th October before dissipating on 19th October at 50.7 N; 45 W. Based on the spatio-temporal information of the two cyclones, the simulations are carried out for H-pol and V-pol BT corresponding to AQUARIUS specifications. The input dataset which includes the vertical profiles of temperature

and relative humidity and surface parameters of SST and WS is prepared on the basis of origin, dissipation time and locations of the cyclones. For the dataset preparation, NCEP GFS analyses fields at 0.5^o spatial resolution and with time interval of every 6 hrs. are extracted over the latitude-longitude domain of 11 N-15 N and 47 E-62 E from 28th October 2015 to 3rd November 2015 for CHAPALA cyclone. For GONZALO, the model domain is selected from 10 N - 55 N and 30 W - 80 W from 20th October 2014 to 25th October 2014. The sea surface salinity during simulation is varied from 10 psu-30 psu at 0.1 psu interval. The noise equivalent delta temperature (NEDT) of an individual sample for Aquarius is 0.15 K [16]. Therefore, a Gaussian random number is generated using the NEDT of Aquarius radiometer and added to the RTM simulated BT values. The NEDT describes the sensitivity of a radiometer in detecting the minimum variations in BT of the scene being observed. The addition of NEDT of the radiometer for the AQUARIUS mission to simulations introduces the sensitivity of the radiometer to the simulations, thus, rendering it more realistic of the actual BT observations. In order to distinguish the simulations with NEDT added to it from the one without it, it is appropriate to designate it as 'realistic simulations'.

4. DEVELOPMENT OF GEOPHYSICAL MODEL FUNCTION

The GMF for WS is based on a multivariate regression model which is a simple linear regression model explaining the relation between the independent variables (predictors) and the dependent variable (criterion) through a best fit line. The linear model is expressed by a mathematical equation using population parameters as

$$Y = a_i X_i + b + \varepsilon, i = 2,..., N \tag{1}$$

Where, X_i is the set of predictor values collected for the regression analysis. In this study, X_i represent the set of BTs- both H-pol ($i = 1$) and V-pol ($i = 2$), simulated for AQUARIUS radiometer measurements for the two cyclonic cases of GONZALO and CHAPALA during the time period of their existence. Y is the set of WS values from NCEP GFS analyses fields which are collocated to the cyclones locations and time. a_i is the slope of the best straight line fit to the match-up data and, b is the intercept on the Y-axis. Both the coefficients are determined from the regression analysis. ε represents the error for individual data point and is estimated from the distance offset between the data point and the best fit line. Statistically, the best fit line is determined from the least squares error analyses where the variance of the linear fit given by relation (2) is minimized.

$$\sigma_{y-Y}^2 = \frac{1}{N}\sum_{i=1}^{N}\{y_i - (a_i X_i + b + \varepsilon)\} \tag{2}$$

N denotes the number of match-up data points of predictor and criterion. y_i is the

measured value of criterion and the parenthesis term is the predicted value. The minimization of relation (2) with respect to a and b separately yields the two coefficients for the best straight line fit.

The sensitivity of L-band radiometer to high WS during TCs is linked with the formation of foam patches due to breaking of waves in ocean [6], which in turn enhances the microwave emissivity ($e \cong 1$) [1], [24] of the ocean surface. The increase in emissivity enhance BT received by the space borne L-band radiometer. However, the foam layer that generate due to high wind will emit L-band radiations only when it is thicker than ~10cm [6]. The required condition only satisfies when ocean surface WS is greater than 12-13m/s [6]. Therefore, ocean surface WS greater than 12m/s are used in developing the GMF from AQUARIUS L-band radiometer. The increase in AQUARIUS radiometer BT for two polarization states, Hpol and Vpol with the ocean surface WS is shown in Figure 1. Both Hpol and Vpol BTs have exhibit linear relationship with the WS. Using Hpol and Vpol as dependent parameters and WS as an independent parameter, a GMF is developed, which is shown in black solid line along with the variations of Hpol BT (blue line) and Vpol BT (red line) in Figure 1. The developed GMF is then used to estimate ocean surface WS for other independent TCs. Hereafter, the GMF for AQUARIUS is denoted by GMF_AQ. The independent TCs are considered based on availability of satellite BT observations over the cyclonic events during the period when the TCs had peak intensity of WS. Based on the criteria, the performance of GMF_AQ is shown for the two cyclones NURI and NILOFAR.

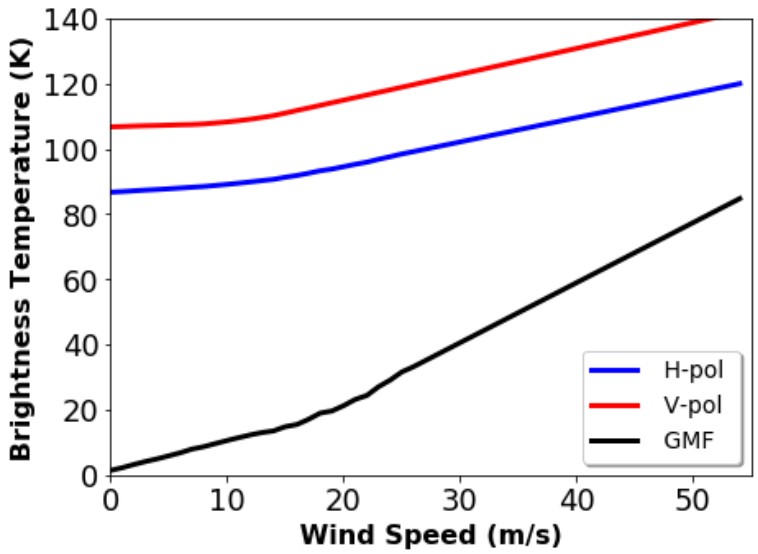

Figure 1. Variations of simulated BT with WS for H-pol (blue line) and V-pol (red line) and the wind speed GMF (black line) for AQUARIUS radiometer.

5. RESULTS AND DISCUSSION

5.1 A brief overview of NURI and NILOFAR cyclones

NURI: NURI was the third most intense TC worldwide in 2014 that developed into a tropical storm on 31st October. It is also known in Philippines as Typhoon Paeng. Due to excellent supporting conditions, NURI underwent rapid deepening to reach its maximum intensity on 2nd November and developed a clear round eye. At this time, Japan Meteorological Agency (JMA) upgraded in into a typhoon. JMA reported a peak intensity with 10-minute maximum sustained winds at 205 km/hr (56.9 m/s; 110.7 kt); its 1-minute maximum sustained winds reaching 285 km/hr (79.2 m/s; 153.8 kt) and Joint Typhoon Warning Centre (JTWC) declared it as a super typhoon. On 3rd November, NURI didn't intensify further and JTWC indicated weakening trend and early on 4th November, JTWC degraded it into a typhoon. Between 5th and 7th November, it was downgraded further into a severe tropical storm at 00 UTC of 6th November and finally into an extra-tropical storm on 7th November.

NILOFAR: NILOFAR originated from the low pressure area between India and Arabian Peninsula in late October of 2014. It was designated a tropical depression on 25th October, 00 UTC by the Indian Meteorological Department (IMD) when it was located at 1270 km southeast of Muscat, Oman. The storm was moving northeast when it strengthened quickly alerting IMD to upgrade it into a deep depression at 03 UTC, cyclonic storm at 06 UTC and a severe cyclonic storm at 21 UTC on 26th October. IMD upgraded it to a very severe cyclonic storm at 06 UTC on 27th October. At 09 UTC on 28th October, IMD upgraded it to an extremely severe tropical cyclone and estimated a 3-minute peak wind of 205 km/hr (56.9 m/s; 110.7 kt) at 18 UTC the same day and JTWC estimated a 1-minute peak wind of 215 km/hr (59.7 m/s; 116.1 kt) at 15 UTC. Thus, NILOFAR was the third strongest storm on record in the Arabian Sea at the time. By 29th October, it started weakening and became a depression by 31st October.

5.2 High Wind Impact on AQUARIUS BT

Figures 2 (a-d) show the spatial distribution of BT obtained from AQUARIUS Level-2 data during TC NURI on 31st October and 3rd November 2014 in the North-Western Pacific Ocean. The left and right panels of the figures show the spatial pattern of H-pol and V-pol BT, respectively. The black dots in the figure show the location of the cyclone on that day. The sea surface roughness effect is more prominent in H-pol compared to V-pol, because H-pol BTs are more affected by the surface roughness compared to V-pol. As the sensor receives more energy with increasing roughness, the BT of both the polarizations continues to rise with the increase in WS. The maximum increase (~6K) in BT of both the polarization is observed on 3rd November 2014 (figs. 2(c-d)) when the TC had intensified to a super typhoon. Thus, the signatures of high ocean winds during TC are very well reflected in the BT values of L-band radiometer data of AQUARIUS.

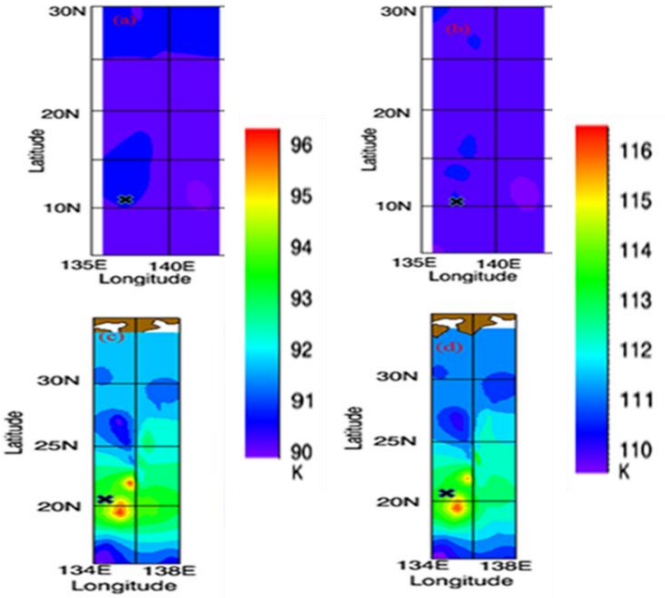

Figure 2. Spatial distribution of BT of AQUARIUS for H-pol (a, c) and V-pol (b, d) during TC NURI on 31st October 2014(a, b) and 3rd November 2014 (c, d).

5.3 Wind Speed Estimation from L-band radiometer for Tropical Cyclones

GMF_AQ given by expression (3) is applied on observed H-pol and V-pol BT from AQUARIUS to estimate the WS during the TCs- NURI (3rd November 2014) and NILOFAR (28th October 2014). For this, the H-pol and V-pol BT from Level-2 data are spatially binned at 0.25° and the GMF_AQ is applied for WS estimation to show the spatial variation in figure 3(a) and 3(b). The WS estimation is done for the date shown in the bracket when high winds were recorded for the cyclones and AQUARIUS observations were concurrently available. The spatial distribution of WS for NURI and NILOFAR are shown in figure 3(a) and 3(b), respectively.

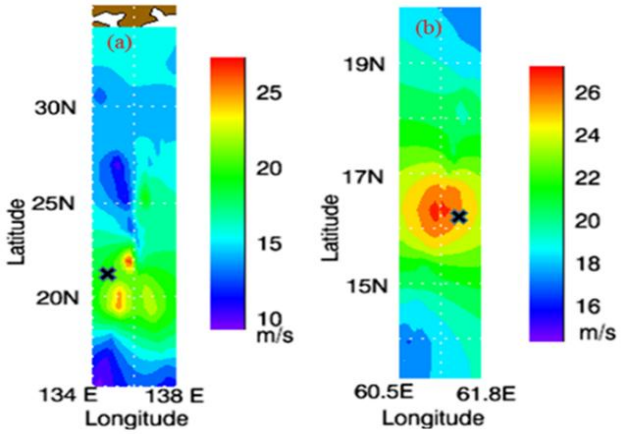

Figure 3. Spatial distribution of estimated WS during TC (a) NURI (3rd November 2014) and (b) NILOFAR (28th October 2014).

The high WS over cyclonic region (black mark) is well captured by the estimations during both the TCs- NURI and NILOFAR, which have been well captured by the small swath (390 km) of AQUARIUS. A scatterplot of the estimated WS against the ancillary WS available with the AQUARIUS Level-2 data is shown in figure 4(a), 4(b) for NURI, NILOFAR respectively. The estimated WS has a standard deviation of 3.2 m/s (2.0 m/s) and correlation coefficient, R of 0.81 (0.91) for NURI (NILOFAR) over a range of WS from 10 m/s to 32 m/s. The combined scatter between estimated and AQUARIUS ancillary WS for two TCs (NURI and NILOFAR) is shown in figure 4(c). The standard deviation of 3.1m/s and R of 0.83 demonstrates the potential of developed GMF in estimating high ocean surface WS during TCs.

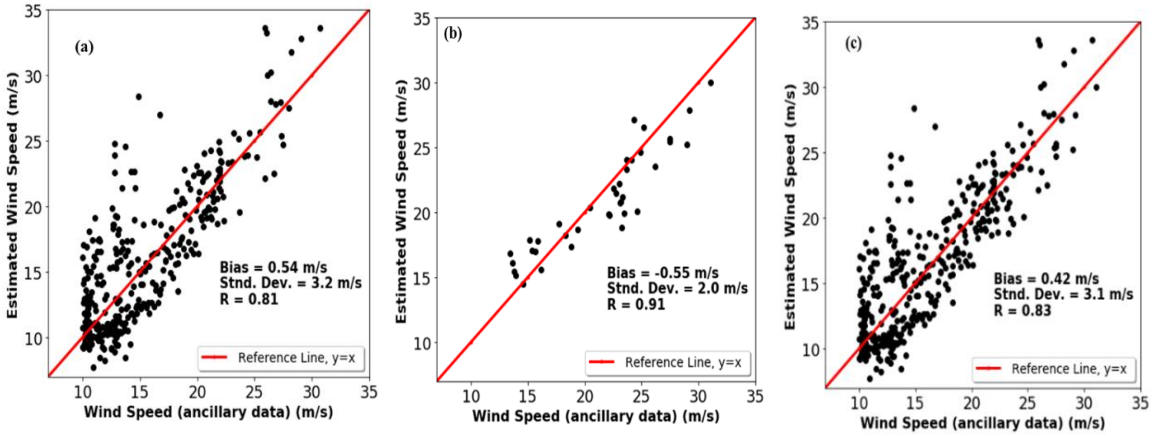

Figure 4. Scatterplot of estimated WS against WS from ancillary data for (a) NURI (b) NILOFAR and (c) combined data of NURI and NILOFAR.

6. CONCLUSIONS

The merits of an L-band radiometer in capturing the severe wind conditions in the presence of heavy rain needs to be explored as much as possible to harness operational benefits from such an instrument. This study follows in the trail of a few similar studies on L-band instrument for wind speed elsewhere. In this work, the wind GMF is developed from simulations for the real cases of TCs for L-band radiometers that existed on AQUARIUS. For realistic simulations, the NEDT of AQUARIUS L-band radiometer is considered. The behavior of simulated BT with WS is shown to be bilinear over two wind regimes. The GMFs are based on bivariate regression model establishing the linear relationship between BT and WS. The GMF_AQ is tested on the TCs NURI and NILOFAR. The spatial variation of BT with high wind conditions are well captured for the AQUARIUS mission over both the cyclonic cases. Scatterplot for estimated WS shows a consistent performance over the moderately high wind range of 12 m/s to 32 m/s for NURI and NILOFAR with a standard deviation of 3.1m/s and R of 0.83.

ACKNOWLEDGEMENTS

Authors would like to thank the Director, Space Applications Centre; Deputy Director, Earth, Ocean, Atmosphere, Planetary Sciences and Applications Area; Group Director, Atmospheric and Oceanic Sciences Group and Head, Geophysical Parameter Retrievals Division for their support and encouragement. Aquarius BT data from Physical Oceanography Distributed Active Archive Centre (PODAAC) maintained by JPL/NASA (ftp://podaac-ftp.jpl.nasa.gov/allData/Aquarius/L2/V4) and GFS analysis fields obtained from www.ncdc.noaa.gov are thankfully acknowledged.

REFERENCES

[1] **Meissner, T. and F. J. Wentz**, 2008, "Wind retrievals under rain for passive satellite microwave radiometers and its application to hurricane tracking," *Proc. IGARSS.*

[2] **Portabella, M., A. Stoffelen, W. Lin, A. Turiel, A. Verhoef, J. Verspeek, and J. Ballabera-Poy**, 2012, "Rain effects on ASCAT-retrieved winds: Toward an improved quality control," *IEEE Trans. Geosci. Rem. Sens., 50(7), 2495-2506, doi: 10.1109/TGRS.2012.2185933.*

[3] **Weissman**, **D., and M. Bourassa**, 2008, "Measurements of the effect of rain-induced sea surface roughness on the QuikSCAT scatterometer radar cross Section," *IEEE Trans. Geosci. Rem. Sens*. 46(10), 2882-2894, doi: 10.1109/TGRS.2008.2001032.

[4] **Ulaby, F. T., R. K. Moore and A. K. Fung**, 1986, Microwave Remote Sensing Active and Passive, From Theory to Applications, *Norwood: Artech House,* Vol.3.

[5] **Hwang**, **P. A.,** 2012, "Foam and roughness effects on passive microwave remote sensing of the ocean," *IEEE Trans*. *Geosci*. *Remote Sens*., 50 (8), 2 978-2 985.

[6] **Reul**, **N., J. Tenerelli, B. Chapron, D. Vandemark, Y. Quilfen and Y. Kerr**, 2012, "SMOS satellite L-band radiometer: A new capability for ocean surface remote sensing in hurricanes," *J. Geophys. Res.*, vol. 117, c02006, doi:10.1029/2011JC007474.

[7] **Reul, N., B. Chapron, E. Zabolotskikh, C. Donlon, Yves. Quilfen, S. Guimbard and J. F. Piolle**, 2016, "A revised L-band radio-brightness sensitivity to extreme winds under tropical cyclones: The 5 year SMOS –Storm database," *Remote Sensing of Environment*, vol. 180, 274-291.

[8] **Le Vine, D. M., G. S. E. Lagerloef and S. E. Torrusio**, 2010, "Aquarius and remote sensing of sea surface salinity from space," *Proceedings of the IEEE*, 98 (5), 688-703.

[9] **Skou**, **N.,** 2004, "Spaceborne L-band Radiometere: Push-broom or Syntehtic Aperture?," *In Proceedings of IGARSS'04 IEEE*, doi:10.1109/IGARSS.2004.1368646.

[10] **Wang, J., J. Zhang, C. Fan and Jing. Wang**, 2015, "A new algorithm for sea-surface wind-speed retrieval based on the L-band radiometer onboard Aquarius," *Chinese J. of Oceanology. and Limnology.,* Vol. 33, Issue 5, pp. 1115–1123.

[11] **Yueh, S., et al.**, 2013, "L-band passive and active microwave geophysical model functions of ocean surface winds and applications to Aquarius retrieval," *IEEE Trans. Geosci. Remote Sens*., Vol. 51, no. 9, pp. 4619-4632.

[12] **Fore, A. G., S. H. Yueh, W. Tang, B. W. Stiles and A. K. Hayashi**, 2016, "Active passive retrievals of ocean winds and sea surface salinity with SMAP," *IEEE Trans. Geosci. Remote Sens.,* Vol. 54, no. 12.

[13] **Meissner, T., L. Ricciardulli, and F. Wentz**, 2017, "Capability of the SMAP Mission to Measure Ocean Surface Winds in Storms," *Bull. Amer. Meteor. Soc.* doi:10.1175/BAMS-D-16-0052.1, in press.

[14] **Sharma, N.,** 2018, "A new approach for estimating ocean surface wind speed using SMAP L-band radiometer," *Weather.* Doi: 10.1002/wea.3415 (in press).

[15] **Kerr**, **Y. H., P. Waldteufel, J. P. Wigneron, S. Delwart, F. Cabot, J. Boutin, M. J. Escorihuela, J. Font, N. Reul, C. Gruhier, S. E. Juglea, M. R. Drinkwater, A. Hahne, M. M. Neira and S. Mecklenburg,** 2010, "The SMOS Misiion: New Tool for Monitoring Key Elements of the Global Water Cycle," *Proceedings of the IEEE,* Vol. 98, No. 5, May 2010, 666-687.

[16] **Piepmeier, J. R., L. Hong, and F. A. Pellerano,** 2015, "Aquarius L-Band Microwave Radiometer: 3 Years of Radiometric Performance and Systematic Effects," *IEEE JSTARS,* Vol. 8, No. 12, December 2015, 5416-5423.

[17] **Piepmeier, J. R., P. Focardi, K. A. Horgan, J. Knuble, N. Ehsan, J. Lucey, C. Brambora, P. R. Brown, P. J. Hoffman, R. T. French, R. L. Mikhaylov, E. Y. Kwack, E. M. Slimko, D. E. Dawson, D. Hudson, J. Peng, P. N. Mohammed, G. D. Amici, A. P. Freedman, J. Medeiros, F. Sacks, R. Estep, M. W. Spencer, C. W. Chen, K. B. Wheeler, W. N. Edelstein, P. E. O'Neill and E. G. Njoku**, 2017, "SMAP L-Band Microwave Radiometer: Instrument Design and First Year on Orbit," *IEEE Trans. Geosci. Rem. Sens.*, Vol. 55, No. 4, 1954-1966.

[18] **Hong, S. and I. Shin,** 2013, "Wind speed retrieval based on sea surface roughness measurements from spaceborne microwave radiometers," *J. Appl. Meteor. Climatol.,* 52, 507-516, doi:10.1175/JAMC-D-11-0209.1.

[19] **Hong, S., H. –J. Seo, N. Kim and I. Shin,** 2015, "Physical retrieval of tropical ocean surface wind speed under rain-free conditions using spaceborne microwave radiometers," *Remote Sens. Lett.*, 6, 380-389, doi:10.1080/2050704X.2015.1037466.

[20] **Kummerow, C.,** 1993, "On the Accuracy of the Eddington Approximation for Radiative Transfer in the Microwave Frequencies," *J. Geophys. Res.*, 98, no. D2, 2757-2765.

[21] **Dave, K.,** 1995, "Refinement of semi empirical model for the microwave emissivity of the sea surface as a function of wind," *Thesis Texas*, A6M University, Report no. 95-090.

[22] **Rosenkranz, P. W.,** 1998, "Water vapor microwave continuum absorption: A comparison of measurements and models," *Radio Science.* 33, 919-928.

[23] **Liebe, H., P. Rosenkranz and G. Hufford,** 1992, "Atmospheric 60-GHz oxygen spectrum: New laboratory measurements and line parameters," *J. Quant. Spectrosc*. Radiat. Transf., 48, 629–643.

[24] **Yueh, S. H., S. J. Dinardo, A. G. Fore, and F. K. Li,** 2010, "Passive and active L-band microwave observations and modeling of ocean surface winds," *IEEE Trans. Geosci. Remote Sens.*, 48(8), 3087–3100, doi:10.1109/TGRS.2010.2045002.